1   Drug synergy of combinatory treatment with remdesivir and the repurposed drugs fluoxetine

2   and itraconazole effectively impairs SARS-CoV-2 infection in vitro.

3   Sebastian Schloer[1], Linda Brunotte[2], Angeles Mecate-Zambrano[2], Shuyu Zheng[3], Jing

4   Tang[3], Stephan Ludwig[2], Ursula Rescher[1]*

5   [1]Institute of Medical Biochemistry, Center for Molecular Biology of Inflammation, and "Cells

6   in Motion" Interfaculty Centre, University of Muenster, Von-Esmarch-Str. 56, D-48149,

7   Muenster, Germany

8   [2]Institute of Molecular Virology, Center for Molecular Biology of Inflammation, and "Cells in

9   Motion" Interfaculty Centre, University of Muenster, Von-Esmarch-Str. 56, D-48149,

10   Muenster, Germany

11   [3]Research Program in Systems Oncology, Faculty of Medicine, University of Helsinki,

12   Haartmaninkatu 8, 00029, Helsinki, Finland

13   *Correspondence: Ursula Rescher, rescher@uni-muenster.de, Tel. +492518352118, Fax.

14   +492518356748

15   running title: Combinatory drug treatment targeting both virus and host-factors to inhibit

16   SARS-CoV-2 infection

17   **ABSTRACT**

18   The SARS-COV-2 pandemic and the global spread of coronavirus disease 2019

19   (COVID-19) urgently calls for efficient and safe antiviral treatment strategies. A

20   straightforward approach to speed up drug development at lower costs is drug repurposing.

21   Here we investigated the therapeutic potential of targeting the host- SARS-CoV-2 interface

22   via repurposing of clinically licensed drugs and evaluated their use in combinatory

23   treatments with virus- and host-directed drugs. We tested the antiviral potential of

24   repurposing the antifungal itraconazole and the antidepressant fluoxetine on the production

25   of infectious SARS-CoV-2 particles in the polarized Calu-3 cell culture model and evaluated

26   the added benefit of a combinatory use of these host-directed drugs with remdesivir, an

27   inhibitor of viral RNA polymerase. Drug treatments were well-tolerated and potent impaired

28   viral   replication   was   observed   with   all   drug   treatments.   Importantly,   both

29   itraconazole-remdesivir and fluoxetine-remdesivir combinations inhibited the production of

30   infectious SARS-CoV-2 particles > 90% and displayed synergistic effects in commonly used

31   reference models for drug interaction. Itraconazole-Remdesivir and Fluoxetine-Remdesivir

32   combinations are promising therapeutic options to control SARS-CoV-2 infection and severe

33   progression of COVID-19.

34   **1. INTRODUCTION**

35   The zoonotic coronavirus SARS-CoV-2 and the resulting COVID-19 pandemic impressively

36   show the global threat potential of a newly emerging pathogen. More than one million people

37   have died so far from the current outbreak, and the proportion of infected people was

38   estimated to reach more than 10% of the global population, with still unknown fatality rates

39   (Baud et al., 2020; Rajgor et al., 2020; Wu et al., 2020). Because of the pressing burden on

40   national health systems and economic losses, safe and efficient treatment strategies are

41   urgently required. Developing a vaccine is a high priority. However, the rigorous testing and

42   extensive clinical trials are time-consuming processes. While several trials are already

43   ongoing, there are no vaccines available yet, and the required widespread access remains a

44   challenging future task. Thus, approaches other than immunization might offer useful

45   additional options for the management and control of SARS-CoV-2 infection and the

46   treatment of COVID-19 (Fierabracci et al., 2020). A possibility to speed up the availability of

47   drugs for the treatment of novel infections is the use of drugs that are already in clinical use

48   for unrelated diseases via so-called "drug repurposing". This approach represents a

49   promising strategy to identify antiviral drugs with faster clinical implementation and lower

50   development costs, considerations that are especially important in the global COVID-19

51   pandemic (Pushpakom et al., 2018). In addition to drugs that directly target the virus, host

52   cell components that are vitally important in the viral life cycle are explored as promising

53   starting points for therapeutic intervention ("host cell-directed therapy") (Schwegmann and

54   Brombacher, 2008; Ianevski et al., 2020; Zumla et al., 2020).

55   Although proteolytic cleavage of the SARS-CoV-2 spike protein surface protein by the host

56   cell transmembrane protease serine 2 (TMPRSS2) enables SARS-CoV-2 to directly fuse

57   with the plasma membrane, endocytosed SARS-CoV-2 particles use endosome-residing

58   proteases for fusion within endosomes (Tang et al., 2020). Both pathways contribute to the

59   SARS-CoV-2 infection process, and the preferential use of the actual fusion pathway might

60   critically depend on the presence of plasma membrane proteases (Hoffmann et al., 2020).

61   Our earlier research on influenza virus infection identified the late endosomal cholesterol

62   balance as a critical factor in the influenza infection success and established this viral entry

63   point as a possible pharmacological target. Elevated cholesterol levels inhibit the fusion of

64   the influenza lipid hull with the endosomal membranes and thus inhibit the efficient transfer

65   of the viral genome into the host cytosol (Musiol et al., 2013; Kühnl et al., 2018). We found

66   that the clinically licensed antifungal itraconazole, a triazole derivative that blocks the fungal

67   ergosterol pathway, has antiviral properties against a range of viruses and is effective

68   against IAV infections in a preclinical mouse model (Schloer et al., 2019, 2020b). The

69   additional therapeutic function is most likely based on direct inhibition of the endosomal

70   cholesterol transporter Niemann-Pick Type C1 (NPC1) and the subsequent cholesterol

71   storage ((Trinh et al., 2017; Schloer et al., 2019)).

72   The late endosome is an entry site for many zoonotically transmitted viruses, in particular for

73   enveloped viruses including SARS-CoV-2 (Tang et al., 2020). Because of the functional

74   similarities in transmitting the viral genome into the host cell, the same endosomal

75   components might serve as pharmacological targets for a broad host-directed antiviral

76   strategy against such viruses. Continuing our work on the endosomal host-virus interface,

77   we explored whether a similar repurposing strategy could be used to impair SARS-CoV-2

78   entry and infection. Therefore, we assessed clinically licensed drugs that also affect

79   endolysosomal lipid storage and cholesterol build-up for their antiviral potential. Here we

80   report that itraconazole treatment potently inhibited the production of SARS-CoV-2

81   infectious particles. Together with our recently published work on the antiviral potential of the

82   widely used serotonin inhibitor fluoxetine, which also negatively affects endosomal

83   cholesterol release (Kornhuber et al., 2010; Schloer et al., 2020a) on SARS-CoV-2 infection,

84   the results presented in this study strongly argue for the endolysosomal host-SARs-CoV-2

85   interface as a druggable target. However, host-directed drugs will rather suppress infection

86   than completely eradicate the pathogen. The resulting demand for high drug doses and

87   early and prolonged treatment is often associated with poor patient compliance. While drugs

88   directly acting on virus structures are much more likely to completely eliminate the

89   pathogens in shorter treatment time, emerging viral resistance to these antivirals is a major

90   concern, as observed with the influenza neuraminidase inhibitor oseltamivir (Kim et al.,

91   2013). Thus, combination therapies using virus- and host-directed drugs are considered to

92   overcome these shortcomings. The nucleoside analog remdesivir which was originally

93   developed against Ebola (Warren et al., 2016), has antiviral properties with a broad

94   spectrum of activity against a number of RNA viruses and has already been shown to be

95   effective against SARS and Mers-CoV in animal experiments (Sheahan et al., 2017, 2020;

96   Agostini et al., 2018; Pruijssers et al., 2020). When remedesivir is incorporated into the viral

97   RNA, the synthesis is prematurely terminated, and viral replication is inhibited (Gordon et al.,

98   2020). Therefore, we explored combined treatments with remdesivir and the repurposed

99   drugs itraconazole and fluoxetine. Both drug combinations showed stronger antiviral

100 activities against influenza viruses compared to remdesivir monotherapy (Schloer et al.,

101 2020b). Importantly, the antiviral effects of the combined treatments deviated from the

102 expected effects, and pharmacodynamic evaluation via commonly used reference models to

103 study drug interaction revealed synergistic interaction.

104 **2. MATERIALS AND METHODS**

105 **2.1 Cells and SARS-CoV-2 isolate**

106 The human bronchial epithelial cell lines Calu-3 and the Vero E6 cells were cultivated in

107 Dulbecco's modified Eagle's medium (DMEM) with 10% standardized fetal bovine serum

108 (FBS Superior; Merck), 2 mM L-glutamine, 100 U/mL penicillin, 0.1 mg/mL streptomycin,

109 and 1% non-essential amino acids (Merck) in a humidified incubator at 5% CO_2 and 37 °C.

110 Calu-3 monolayers were polarized and cultured as described (Schloer et al., 2020b).

111   Itraconazole (2 mg/mL, Sigma), fluoxetine (5 mM, Sigma) and remdesivir (10 mM, Hycultec)

112   were solubilized in DMSO. The SARS-CoV-2 isolate hCoV-19/Germany/FI1103201/2020

113   (EPI-ISL_463008, mutation D614G in spike protein) was amplified on Vero E6 cells and

114   used for the infection assays.

115   **2.2 Cytotoxicity assay**

116   Calu-3 cells were cultured at the indicated concentrations with either the solvent DMSO,

117   itraconazole or with the combinations of itraconazole/ remdesivir (ItraRem) or fluoxetine/

118   remdesivir (FluoRem) for 48 h. Staurosporine solution (1 µM) served as a positive control for

119   cytotoxic effects. After 48 hours of treatment, cell viability was evaluated by adding MTT

120   3-(4,5-dimethylthiazol-2-yl)-2,5-diphenyltetrazolium bromide (Sigma) to the cells for 4 h and

121   OD_{562} measurements according to the manufacturer's protocols (Sigma).

122   **2.3 Inoculation of cells and drug treatment**

123   For infection, polarized Calu-3 and Vero cells were washed with PBS and inoculated at a

124   multiplicity of infection (MOI) of 0.1 (Calu-3) or 0.01 (Vero E6) of virus diluted in

125   infection-PBS (containing 0.2% BSA, 1% $CaCl_2$, 1% $MgCl_2$, 100 U/mL penicillin and 0.1

126   mg/mL streptomycin) at 37°C for 1 hours. Subsequently, cells were washed with PBS and

127   further cultured in infection-DMEM (serum-free DMEM containing 0.2% BSA, 1 mM $MgCl_2$,

128   0.9 mM $CaCl_2$, 100 U/mL penicillin, and 0.1 mg/mL streptomycin) at 5% CO_2 and 37 °C.

129   Cells were treated with the indicated remdesivir, itraconazole or fluoxetine concentration 2

130   hours post-infection (hpi) for the entire 48 hours infection period. After 48 hpi, apical culture

131   supernatants were collected and immediately frozen at -80 °C until titration via plaque

132   assay.

133   **2.4 Plaque assay**

134   To determine the number of infectious particles in the supernatant of treated cells, a

135   standard plaque assay was performed. Briefly, Vero E6 cells grown to a monolayer in

136   six-well dishes were washed with PBS and infected with serial dilutions of the respective

137   supernatants in infection-PBS for 1 hour at 37 °C. The inoculum was replaced with 2x MEM

138   (MEM containing 0.2% BSA, 2 mM L-glutamine 1 M HEPES, pH 7.2, 7.5% NaHCO$_3$, 100

139   U/mL penicillin, 0.1 mg/mL streptomycin, and 0.4% Oxoid agar) and incubated at 37°C.

140   Virus plaques were visualized by staining with neutral red, and virus titers were calculated as

141   plaque-forming units (PFU) per mL.

142   **2.5 Data and statistical analysis**

143   A priori power analysis using G*Power 3.1 (Faul et al., 2007)) was performed to determine

144   the sample sizes required to detect > 90% reduction in virus titers at powers > 0.8. Data

145   were analyzed using the software GraphPad Prism version 8.00 (GraphPad). No outliers

146   were detected.

147   Infectious viral titers are presented as means ± SEM of five measurements per

148   experiment per condition. For dose-response curves, drug concentrations were

149   log-transformed and virus titers were expressed as percentages of the mean virus titer in

150   control cells (treated with the solvent DMSO) and data were analyzed by curve fitting using a

151   4 parameter logistic model. Drug combinatory effects were analyzed by using

152   SynergyFinder, an open-source free stand-alone web application for the analysis of drug

153   combination data (Ianevski et al., 2017). Synergy was evaluated based on the Zero

154   Interaction Potency (ZIP), Bliss independence, and Highest single agent (HSA) reference

155   models (He et al., 2018). We further analyzed the overall drug combination sensitivity score

156   (CSS) by using the CSS method (Malyutina et al., 2019).

157   **3. RESULTS**

158   **3.1. The clinically licensed antifungal drug itraconazole efficiently blocks the**

159   **production of SARS-CoV-2 infectious particles**

160   Based on the successful use of repurposing itraconazole for the treatment of influenza virus

161   infection reported in our earlier studies (Schloer et al., 2019, 2020b), we first established

162   whether this clinically licensed drug also had an antiviral potential on the production of

163   infectious SARS-CoV-2 particles. In line with our previous results (Schloer et al., 2020a),

164   both Calu-3 and Vero E6 cell lines supported SARS-CoV-2 replication and produced high

165 virus titers (Fig. 1). Inoculation with the clinical isolate hCoV-19/Germany/FI1103201/2020

166 at MOI 0.1 yielded 1.46×10^6 PFU in Calu-3 cells and 6.37×10^6 PFU at MOI 0.01 in Vero cells

167 at 48 hpi. Treatment with itraconazole 2 hpi potently inhibited SARS-CoV-2 replication in a

168 dose-dependent manner in both cell types (Fig. 1a). Fitting the experimental dose-response

169 values to a nonlinear 4 parameter logistic model revealed half-maximal inhibitory (EC_{50}) and

170 90% inhibitory concentrations (EC_{90}) of 0.43 µM and 2.46 µM in Calu-3 cells, and even lower

171 50% and 90% inhibitory concentrations (0.39 µM and 0.87 µM) were determined for

172 itraconazole antiviral activity in SARS-CoV-2 infected Vero cells (Fig. 1b). Of note, no

173 detectable cytotoxicity was observed with these doses (Fig. S1a). The itraconazole cytotoxic

174 concentration required to reduce cell viability by 50% (CC_{50}) was determined at 25.56 µM,

175 resulting in a selectivity index (SI, defined as the ratio of CC_{50} to EC_{50}) of 25.56 µM which

176 indicated an effective and safe antiviral window.
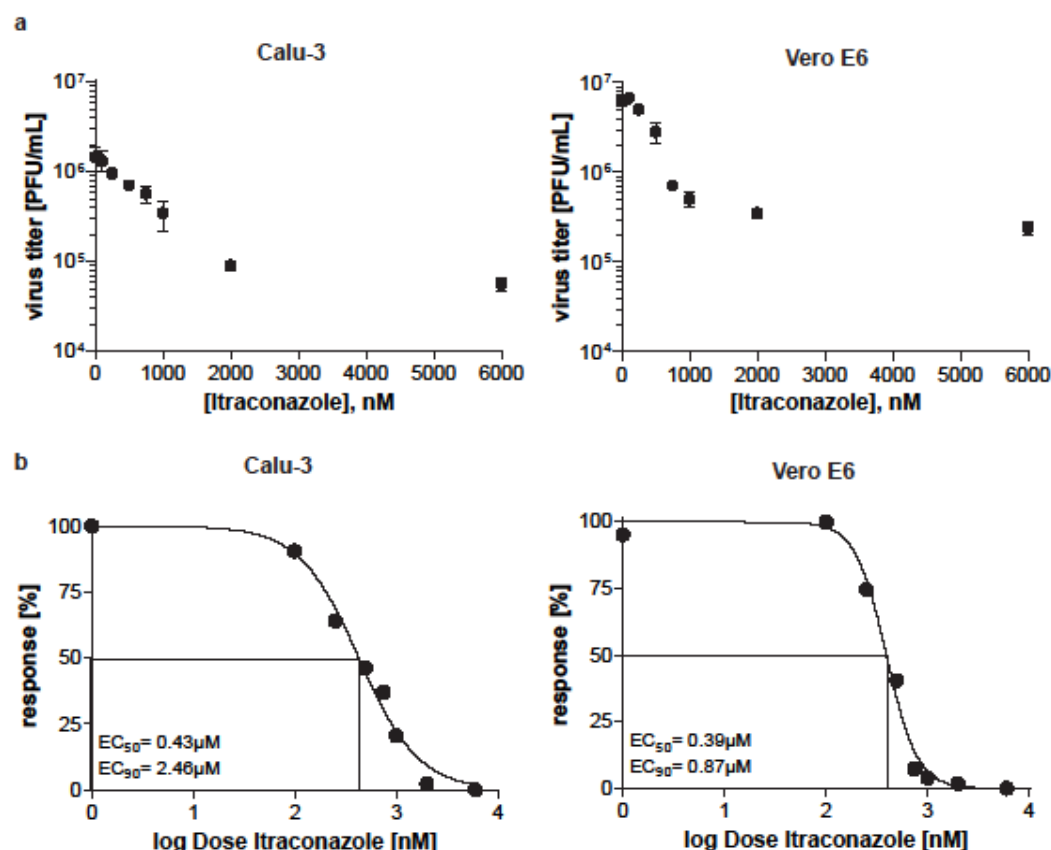
177
178 **FIGURE 1** Analysis of itraconazole-mediated reduction of SARS-CoV-2 replication. Calu-3

179 and Vero E6 cells were infected with 0.1 MOI of SARS-CoV-2. At 2 hpi, cells were treated

180 with itraconazole at the indicated concentrations. (a) Mean infectious viral titers ± SEM,

181   (b) Mean percent inhibition $\pm$ SEM of SARS-CoV-2 replication, with mean virus titer in

182   control cells (treated with the solvent DMSO) set to 100%; n $=$ 5. LogEC$_{50}$ and LogEC$_{90}$

183   values were determined by fitting a non-linear regression model. (Calu-3: EC$_{50}$ = 0.43 µM,

184   EC$_{90}$ = 2.46 µM; Vero E6: EC$_{50}$ = 0.39 µM, EC$_{90}$ = 0.87 µM).

185   **3.2 Remdesivir inhibits SARS-CoV-2 replication in polarized Calu-3 cells**

186   We addressed the question of whether a host-targeting drug could be used in combination

187   with a virus-directed drug for more efficient suppression of SARS-CoV-2 replication. Thus,

188   we first assessed the antiviral capacity of remdesivir, a nucleotide analog prodrug that

189   inhibits SARS-CoV-2 viral RNA-dependent RNA polymerase (Gordon et al., 2020). The

190   EC$_{50}$ concentration was reached at 0.42 µM and EC$_{90}$ at 1.08 µM in Calu-3 cells (Fig. S2),

191   well in line with published data (Pruijssers et al., 2020). Next, we determined viral replication

192   in cells that had been treated with combinatory therapy. Because we recently published the

193   potential use of repurposing the antidepressant fluoxetine for treatment of SARS-CoV-2

194   infection (Schloer et al., 2020a), we also assessed the effects of a combined

195   fluoxetine/remdesivir (FluoRem) treatment in addition to the itraconazole/remdesivir

196   (ItraRem) combination (Fig. 2). Both drugs are clinically licensed and do not induce

197   significant cytotoxicity over the whole concentration range ((Schloer et al., 2020a), and Fig.

198   S1a). The combination treatments were also well-tolerated, and no cytotoxic effects were

199   seen when cells were simultaneously treated with the drug pairs (Fig. S1b, c).
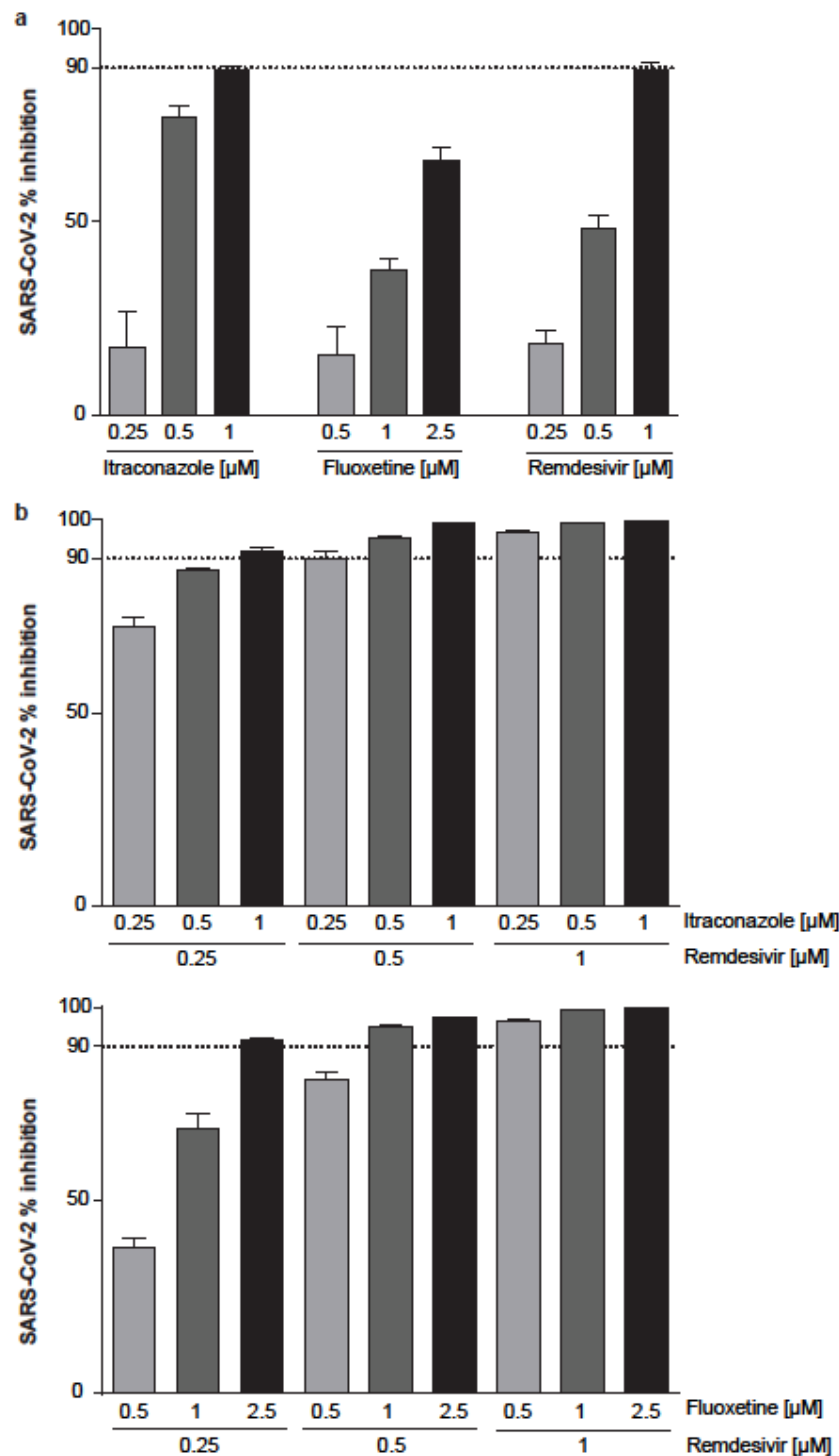
200   **3.3 Combinatory treatments with the drug pairs itraconazole-remdesivir or**

201   **fluoxetine-remdesivir show enhanced antiviral activity due to synergistic interaction**

202   For all drugs, we chose those concentrations that were not sufficient to achieve a 90%

203   reduction when individually applied (Fig 3a). For both ItraRem and FluoRem combinations, a

204   potent reduction in virus titers was detected in all cases. Of note, several combinations

205   yielded a reduction > 90% of the maximum virus titers produced in control cells (Fig. 3b).
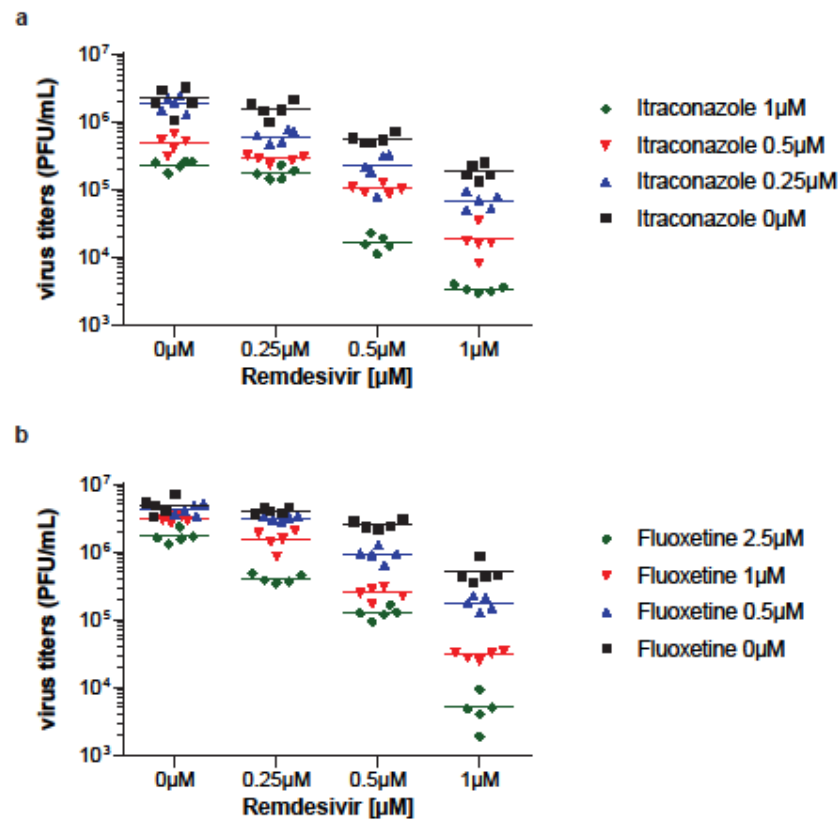
FIGURE 2 Antiviral activities of treatments. Infectious virus production in Calu-3 cells treated as indicated 2 hpi. Each symbol represents plaque-forming units (PFU) per mL detected in a single experimental sample, lines indicate means.
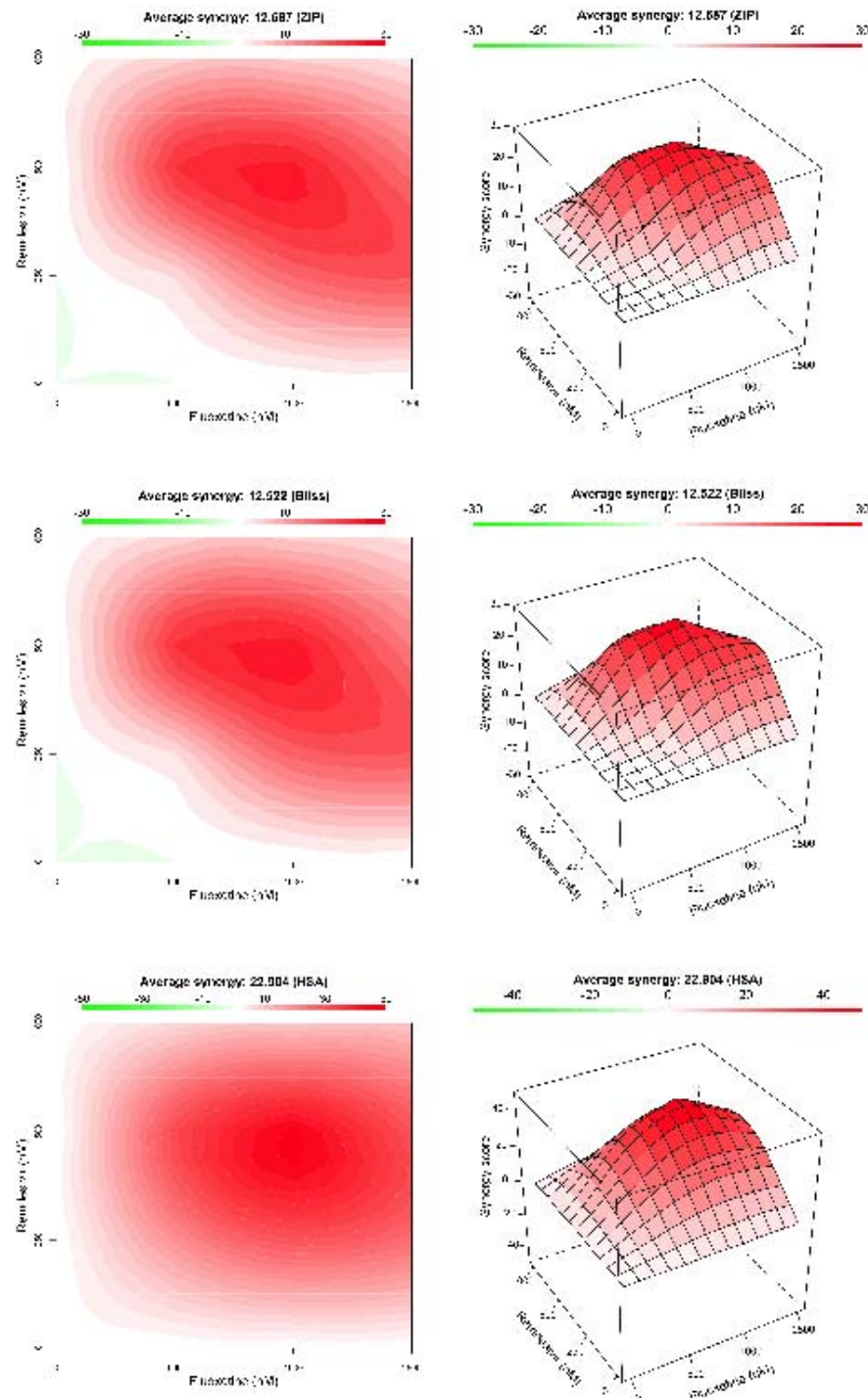
210
211 **FIGURE 3** Antiviral activities of single and combination treatments. Calu-3 cells were treated

212 with the indicated drug combinations for 48 h. (a) Single treatment, (b) combinatory

213 treatment. Bars represent mean percent inhibition ± SEM of infectious virus production,

214 with mean virus titer produced in control cells (treated with the solvent DMSO) set to 100%;

215 n = 5. Dotted line, 90% reduction in viral titer.

216   We, next considered the pharmacological interactions of the respective drug pairs. Thus, we

217   evaluated the drug interactions via Bliss independence, Highest single agent (HSA), and

218   ZIP, three commonly used reference synergy models that differ in their basic assumptions of

219   drug interaction they are based on. The results, presented in Figs. 4 and 5, consistently

220   argued for synergistic action of remdesivir with itraconazole and fluoxetine, as indicated by

221   the positive average synergy score across all models. Closer inspection of the drug

222   interaction relationships and landscape visualizations revealed that for ItraRem, the highest

223   synergy scores were calculated with the lower concentration ranges of both drugs (Fig. 4).

224   The strong synergy led to an overall drug combination sensitivity score (CSS) of 89.64,

225   resulting in >90% inhibition already at 500 nM of remdesivir and 250 nM of itraconazole.

226   FluoRem combination treatment had a higher average synergy score, as well as a higher

227   CSS score than ItraRem (92.82 vs 89.64), suggesting that this drug combination is more

228   likely to show synergy. Importantly, for all models, the FluoRem combinations that met the ≥

229   90% inhibition criterion were well within the high synergy area (Fig. 5).

230 **Figure**
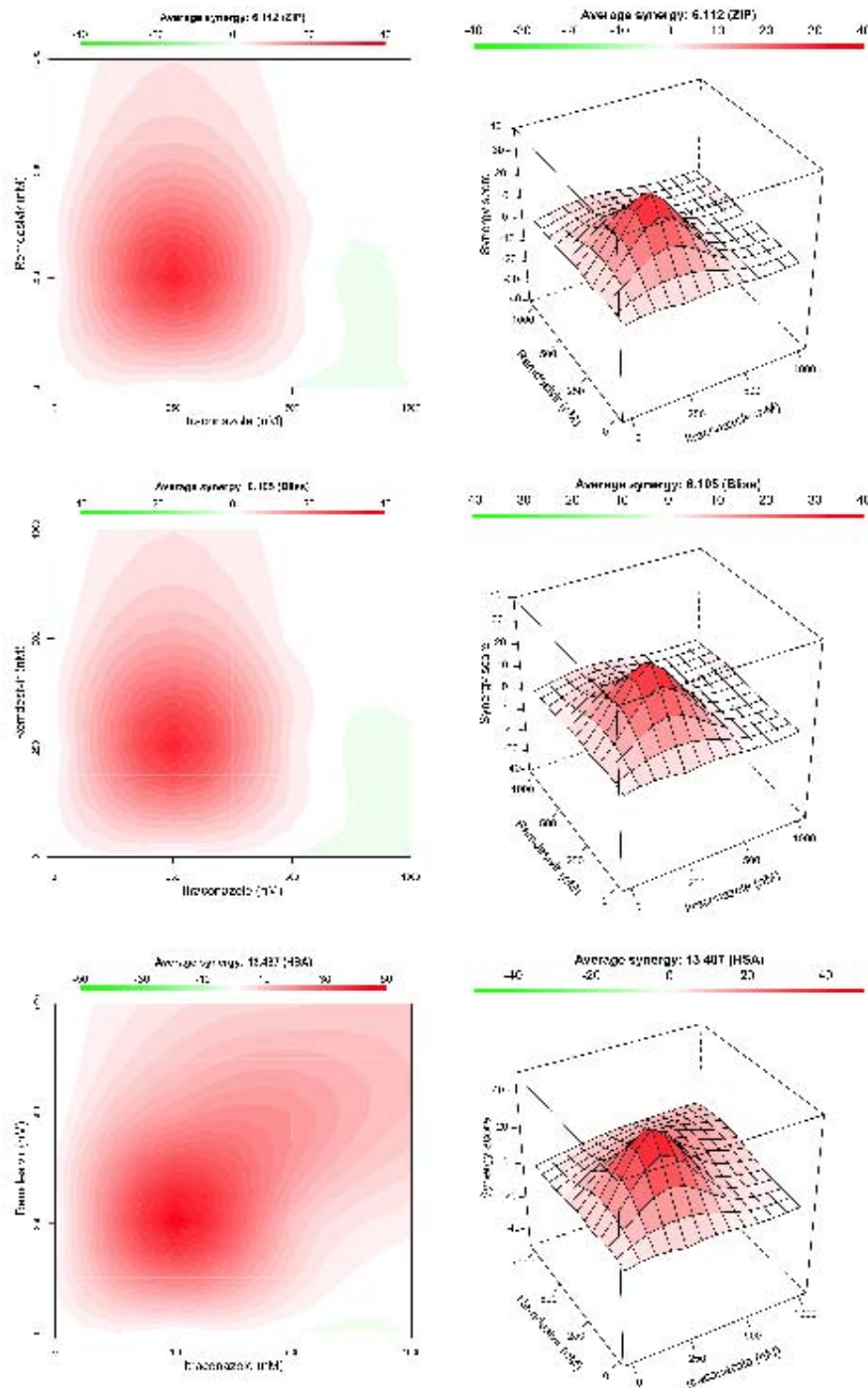
231   **FIGURE 4.** Evaluation of the pharmacological interactions of itraconazole and remdesivir

232   (ItraRem). ZIP, Bliss independence, and Highest single agent (HSA) reference models were

233   used to assess the interaction landscapes. Interaction surfaces are color-coded according to

234   the synergy scores of the responses.

235
236 **FIGURE 5.** Evaluation of the pharmacological interactions of fluoxetine and remdesivir

237 (FluoRem). ZIP, Bliss independence, and Highest single agent (HSA) reference models

238 were used to assess the interaction landscapes. Interaction surfaces are color-coded

239 according to the synergy scores of the responses.

240 **4. DISCUSSION**

241 The nucleoside analog remdesivir with broad-spectrum antiviral activity against a range of

242 viruses including Ebola, Marburg, MERS, and SARS inhibits viral RNA polymerase and is

243 also active against SARS-CoV-2 (Warren et al., 2016; Sheahan et al., 2017, 2020; Agostini

244 et al., 2018; Brown et al., 2019). Indeed, remedesivir was the first new drug to receive an

245 FDA emergency use authorization for the treatment of severe COVID-19 cases. However, a

246 common concern about virus-directed antivirals is the development of drug resistance. Due

247 to their error-prone replication mode, drug-resistant viruses are increasingly encountered

248 (Strasfeld and Chou, 2010), as observed with the influenza neuraminidase inhibitor

249 oseltamivir (Kim et al., 2013). Because profound changes would be required to allow viruses

250 to replicate independently of otherwise essential host factors, the development of

251 host-directed therapeutics is an emerging concept. However, host-directed drugs will rather

252 cause impaired viral replication than complete eradication, thus demanding high drug

253 concentrations and starting treatment start as early as possible and for extended durations,

254 which is often associated with poor patient compliance. Because of these shortcomings,

255 combinatory treatments with both virus- and host-directed drugs are explored for enhanced

256 treatment success.

257 Enveloped viruses such as SARS-CoV-2 depend on the fusion of their lipid hull with the host

258 membrane to get access to the cytosol. The SARS-CoV-2 spike protein, which protrudes

259 from the virus surface, mediates initial binding to angiotensin-converting enzyme 2 (ACE2),

260 which serves as the host cell surface receptor (Li et al., 2003; Lan et al., 2020; Ou et al.,

261 2020; Zhou et al., 2020). To promote fusion with the host cell membrane, the spike protein

262 needs to be primed by proteolytic cleavage, which can be mediated by several host

263 proteases. Transmembrane protease serine 2 (TMPRSS2)-mediated cleavage leads to

264 fusion with the plasma membrane, while endosome-residing proteases are utilized by

265 endocytosed SARS-CoV-2 particles for fusion within endosomes. Since both routes have

266 been reported to contribute to the SARS-CoV-2 infectivity (Hoffmann et al., 2020), the

267 endosomal compartment is also a critical host/pathogen interface for SARS-CoV-2. Our

268 previous studies strongly support the late endosomal cholesterol balance as a cellular target

269   for antiviral intervention (Musiol et al., 2013; Kühnl et al., 2018; Schloer et al., 2019, 2020a,

270   2020b). Notably, endolysosomal lipid storage and cholesterol build-up could be induced via

271   repurposing of drugs approved for unrelated applications. We found that the triazole

272   derivative itraconazole, a clinically licensed antifungal drug (Organization, 2019) that directly

273   inhibits the endosomal cholesterol transporter NPC1 (Trinh et al., 2017) has an antiviral

274   potential on the endosomal fusion of enveloped viruses including influenza viruses (Schloer

275   et al., 2019). The findings presented in this study add SARS-CoV-2 to the spectrum of

276   itraconazole-sensitive enveloped viruses. Our results reveal a potent antiviral activity of

277   itraconazole on the production of SARS-CoV-2 infectious particles, with EC_{50} values

278   comparable to what we previously reported for itraconazole-mediated antiviral activity

279   against IAV subtypes. The bioavailability after oral application of itraconazole is low because

280   of the low water solubility of this compound (Grant Prentice and Glasmacher, 2005;

281   Domínguez-Gil Hurlé et al., 2006). Only limited amounts are absorbed from the

282   gastrointestinal tract after ionization, and levels depend on the individual gastric acidity (Shin

283   et al., 2004; Domínguez-Gil Hurlé et al., 2006; Bae et al., 2011; Lestner and Hope, 2013;

284   Allegra et al., 2017). However, our previous study revealed a beneficial antiviral activity in

285   vivo (Schloer et al., 2019).

286   We recently discovered that the widely used antidepressant fluoxetine has strong

287   SARS-CoV-2 antiviral activity (Schloer et al., 2020a). Together with the findings presented

288   here on the inhibitory function of itraconazole treatment on SARS-CoV-2 replication, these

289   results suggest that both drugs are promising candidates for repurposing as a host-directed

290   drug for SARS-CoV-2 infection treatment. Both drugs most likely interfere with the proper

291   endosomal cholesterol levels. Whereas itraconazole und posaconazole both directly inhibit

292   the endosomal cholesterol transporter NPC1 (Trinh et al., 2017), fluoxetine functionally

293   blocks the endolysosome-residing enzyme sphingomyelin phosphodiesterase ("acid

294   sphingomyelinase", ASM), which in turn causes sphingomyelin accumulation and negatively

295   affects cholesterol release from this compartment (Kornhuber et al., 2010).

5. CONCLUSION

While remdesivir and the host-directed drugs itraconazole or fluoxetine target independent pathways, we found that drug combinations together with remdesivir (ItraRem and FluoRem) showed stronger antiviral activities against SARS-CoV-2 than the remdesivir monotherapy. Moreover, the overall therapeutic effect of the combinations was larger than the expected sum of the independent drug effects. Our analysis on the antiviral activity of combinatory drug combinations via commonly used interaction models argue for an enhanced efficacy that is based on synergistic drug interaction and suggests promising novel options for SARS-CoV-2 treatment.

CONFLICT OF INTEREST

The authors declare no conflict of interest. The funders had no role in the design of the study; in the collection, analyses, or interpretation of data; in the writing of the manuscript, or in the decision to publish the results.

AUTHOR CONTRIBUTIONS

322 Conceptualization and methodology, S.S., U.R.; validation, formal analysis, investigation,

323 data curation, S.S., J.T., U.R.; resources, J.T., S.L.; U.R.; writing—original draft preparation,

324 U.R.; writing—review and editing, S.S., S.L., U.R.; visualization, S.S.; supervision, U.R.,

325 S.L., project administration, U.R.; funding acquisition, U.R. All authors have read and agreed

326 to the published version of the manuscript.

327 **REFERENCES**

328 Agostini, M.L., Andres, E.L., Sims, A.C., Graham, R.L., Sheahan, T.P., Lu, X., et al. (2018).

329   Coronavirus susceptibility to the antiviral remdesivir (GS-5734) is mediated by the viral

330   polymerase and the proofreading exoribonuclease. MBio *9*: 2020.

331 Allegra, S., Fatiguso, G., Francia, S. De, Favata, F., Pirro, E., Carcieri, C., et al. (2017).

332   Evaluation of posaconazole pharmacokinetics in adult patients with invasive fungal

333   infection. Biomedicines *5*:.

334 Bae, S.K., Park, S.-J., Shim, E.-J., Mun, J.-H., Kim, E.-Y., Shin, J.-G., et al. (2011).

335   Increased Oral Bioavailability of Itraconazole and Its Active Metabolite,

336   7-Hydroxyitraconazole, When Coadministered With a Vitamin C Beverage in Healthy

337   Participants. J. Clin. Pharmacol. *51*: 444–451.

338 Baud, D., Qi, X., Nielsen-Saines, K., Musso, D., Pomar, L., and Favre, G. (2020). Real

339   estimates of mortality following COVID-19 infection. Lancet Infect. Dis. *20*: 773.

340 Brown, A.J., Won, J.J., Graham, R.L., Dinnon, K.H., Sims, A.C., Feng, J.Y., et al. (2019).

341   Broad spectrum antiviral remdesivir inhibits human endemic and zoonotic

342   deltacoronaviruses with a highly divergent RNA dependent RNA polymerase. Antiviral

343   Res. *169*:.

344 Domínguez-Gil Hurlé, A., Sánchez Navarro, A., and García Sánchez, M.J. (2006).

345   Therapeutic drug monitoring of itraconazole and the relevance of pharmacokinetic

346   interactions. Clin. Microbiol. Infect. *12*: 97–106.

347   Faul, F., Erdfelder, E., Lang, A.-G., and Buchner, A. (2007). G*Power 3: A flexible statistical
348   power analysis program for the social, behavioral, and biomedical sciences. Behav.
349   Res. Methods *39*: 175–191.

350   Fierabracci, A., Arena, A., and Rossi, P. (2020). COVID-19: A review on diagnosis,
351   treatment, and prophylaxis. Int. J. Mol. Sci. *21*: 1–16.

352   Gordon, C.J., Tchesnokov, E.P., Woolner, E., Perry, J.K., Feng, J.Y., Porter, D.P., et al.
353   (2020). Remdesivir is a direct-acting antiviral that inhibits RNA-dependent RNA
354   polymerase from severe acute respiratory syndrome coronavirus 2 with high potency. J.
355   Biol. Chem. *295*: 6785–6797.

356   Grant Prentice, A., and Glasmacher, A. (2005). Making sense of itraconazole
357   pharmacokinetics. J. Antimicrob. Chemother. *56*: 17–22.

358   He, L., Kulesskiy, E., Saarela, J., Turunen, L., Wennerberg, K., Aittokallio, T., et al. (2018).
359   Methods for high-throughput drug combination screening and synergy scoring. In
360   Methods in Molecular Biology, (Humana Press Inc.), pp 351–398.

361   Hoffmann, M., Kleine-Weber, H., Schroeder, S., Krüger, N., Herrler, T., Erichsen, S., et al.
362   (2020). SARS-CoV-2 Cell Entry Depends on ACE2 and TMPRSS2 and Is Blocked by a
363   Clinically Proven Protease Inhibitor. Cell *181*: 271–280.e8.

364   Ianevski, A., He, L., Aittokallio, T., and Tang, J. (2017). SynergyFinder: A web application for
365   analyzing drug combination dose-response matrix data. Bioinformatics *33*: 2413–2415.

366   Ianevski, A., Yao, R., Fenstad, M.H., Biza, S., Zusinaite, E., Reisberg, T., et al. (2020).
367   Potential antiviral options against SARS-CoV-2 infection. Viruses *12*:.

368   Kim, J.H., Resende, R., Wennekes, T., Chen, H.M., Bance, N., Buchini, S., et al. (2013).
369   Mechanism-based covalent neuraminidase inhibitors with broad-spectrum influenza
370   antiviral activity. Science (80-.). *340*: 71–75.

bioRxiv preprint doi: https://doi.org/10.1101/2020.10.16.342410; this version posted October 16, 2020. The copyright holder for this preprint (which was not certified by peer review) is the author/funder, who has granted bioRxiv a license to display the preprint in perpetuity. It is made available under aCC-BY-NC-ND 4.0 International license.

371   Kornhuber, J., Tripal, P., Reichel, M., Mühle, C., Rhein, C., Muehlbacher, M., et al. (2010).

372   Functional Inhibitors of Acid Sphingomyelinase (FIASMAs): A Novel Pharmacological

373   Group of Drugs with Broad Clinical Applications.

374   Kühnl, A., Musiol, A., Heitzig, N., Johnson, D.E., Ehrhardt, C., Grewal, T., et al. (2018). Late

375   endosomal/lysosomal cholesterol accumulation is a host cell-protective mechanism

376   inhibiting endosomal release of influenza A virus. MBio *9*: e01345-18.

377   Lan, J., Ge, J., Yu, J., Shan, S., Zhou, H., Fan, S., et al. (2020). Structure of the

378   SARS-CoV-2 spike receptor-binding domain bound to the ACE2 receptor. Nature *581*:

379   215–220.

380   Lestner, J., and Hope, W.W. (2013). Itraconazole: An update on pharmacology and clinical

381   use for treatment of invasive and allergic fungal infections. Expert Opin. Drug Metab.

382   Toxicol. *9*: 911–926.

383   Li, W., Moore, M.J., Vasllieva, N., Sui, J., Wong, S.K., Berne, M.A., et al. (2003).

384   Angiotensin-converting enzyme 2 is a functional receptor for the SARS coronavirus.

385   Nature *426*: 450–454.

386   Malyutina, A., Majumder, M.M., Wang, W., Pessia, A., Heckman, C.A., and Tang, J. (2019).

387   Drug combination sensitivity scoring facilitates the discovery of synergistic and

388   efficacious drug combinations in cancer. PLoS Comput. Biol. *15*:.

389   Musiol, A., Gran, S., Ehrhardt, C., Ludwig, S., Grewal, T., Gerke, V., et al. (2013). Annexin

390   A6-balanced late endosomal cholesterol controls influenza a replication and

391   propagation. MBio *4*: 1–11.

392   Organization, W.H. (2019). World Health Organization Model List of Essential Medicines

393   (Geneve).

394   Ou, X., Liu, Y., Lei, X., Li, P., Mi, D., Ren, L., et al. (2020). Characterization of spike

395   glycoprotein of SARS-CoV-2 on virus entry and its immune cross-reactivity with

396   SARS-CoV. Nat. Commun. *11*: 1–12.

397   Pruijssers, A.J., George, A.S., Schäfer, A., Leist, S.R., Gralinksi, L.E., Dinnon, K.H., et al.

398   (2020). Remdesivir Inhibits SARS-CoV-2 in Human Lung Cells and Chimeric

399   SARS-CoV Expressing the SARS-CoV-2 RNA Polymerase in Mice. Cell Rep. *32*:

400   107940.

401   Pushpakom, S., Iorio, F., Eyers, P.A., Escott, K.J., Hopper, S., Wells, A., et al. (2018). Drug

402   repurposing: Progress, challenges and recommendations. Nat. Rev. Drug Discov. *18*:

403   41–58.

404   Rajgor, D.D., Lee, M.H., Archuleta, S., Bagdasarian, N., and Quek, S.C. (2020). The many

405   estimates of the COVID-19 case fatality rate. Lancet Infect. Dis. *20*: 776–777.

406   Schloer, S., Brunotte, L., Goretzko, J., Mecate-Zambrano, A., Korthals, N., Gerke, V., et al.

407   (2020a). Targeting the endolysosomal host-SARS-CoV-2 interface by clinically licensed

408   functional inhibitors of acid sphingomyelinase (FIASMA) including the antidepressant

409   fluoxetine. Emerg. Microbes Infect. 1–26.

410   Schloer, S., Goretzko, J., Kühnl, A., Brunotte, L., Ludwig, S., and Rescher, U. (2019). The

411   clinically licensed antifungal drug itraconazole inhibits influenza virus *in vitro* and *in vivo*.

412   Emerg. Microbes Infect. *8*: 80–93.

413   Schloer, S., Goretzko, J., Pleschka, S., Ludwig, S., and Rescher, U. (2020b). Combinatory

414   Treatment with Oseltamivir and Itraconazole Targeting Both Virus and Host Factors in

415   Influenza A Virus Infection. Viruses *12*: 703.

416   Schwegmann, A., and Brombacher, F. (2008). Host-directed drug targeting of factors

417   hijacked by pathogens. Sci. Signal. *1*: re8.

418   Sheahan, T.P., Sims, A.C., Graham, R.L., Menachery, V.D., Gralinski, L.E., Case, J.B., et al.

419   (2017). Broad-spectrum antiviral GS-5734 inhibits both epidemic and zoonotic

420   coronaviruses. Sci. Transl. Med. *9*:.

421   Sheahan, T.P., Sims, A.C., Leist, S.R., Schäfer, A., Won, J., Brown, A.J., et al. (2020).

422   Comparative therapeutic efficacy of remdesivir and combination lopinavir, ritonavir, and

423   interferon beta against MERS-CoV. Nat. Commun. *11*: 1–14.

424   Shin, J.H., Choi, K.Y., Kim, Y.C., and Lee, M.G. (2004). Dose-Dependent Pharmacokinetics

425   of Itraconazole after Intravenous or Oral Administration to Rats: Intestinal First-Pass

426   Effect. Antimicrob. Agents Chemother. *48*: 1756–1762.

427   Strasfeld, L., and Chou, S. (2010). Antiviral drug resistance: Mechanisms and clinical

428   implications. Infect. Dis. Clin. North Am. *24*: 809–833.

429   Tang, T., Bidon, M., Jaimes, J.A., Whittaker, G.R., and Daniel, S. (2020). Coronavirus

430   membrane fusion mechanism offers a potential target for antiviral development.

431   Antiviral Res. *178*:.

432   Trinh, M.N., Lu, F., Li, X., Das, A., Liang, Q., Brabander, J.K. De, et al. (2017). Triazoles

433   inhibit cholesterol export from lysosomes by binding to NPC1. Proc. Natl. Acad. Sci.

434   *114*: 89–94.

435   Warren, T.K., Jordan, R., Lo, M.K., Ray, A.S., Mackman, R.L., Soloveva, V., et al. (2016).

436   Therapeutic efficacy of the small molecule GS-5734 against Ebola virus in rhesus

437   monkeys. Nature *531*: 381–385.

438   Wu, J.T., Leung, K., Bushman, M., Kishore, N., Niehus, R., Salazar, P.M. de, et al. (2020).

439   Estimating clinical severity of COVID-19 from the transmission dynamics in Wuhan,

440   China. Nat. Med. *26*: 506–510.

441   Zhou, P., Yang, X. Lou, Wang, X.G., Hu, B., Zhang, L., Zhang, W., et al. (2020). A

442   pneumonia outbreak associated with a new coronavirus of probable bat origin. Nature

443   *579*: 270–273.

444   Zumla, A., Hui, D.S., Azhar, E.I., Memish, Z.A., and Maeurer, M. (2020). Reducing mortality

445   from 2019-nCoV: host-directed therapies should be an option. Lancet *395*: e35–e36.

446 **SUPPORTING INFORMATION**
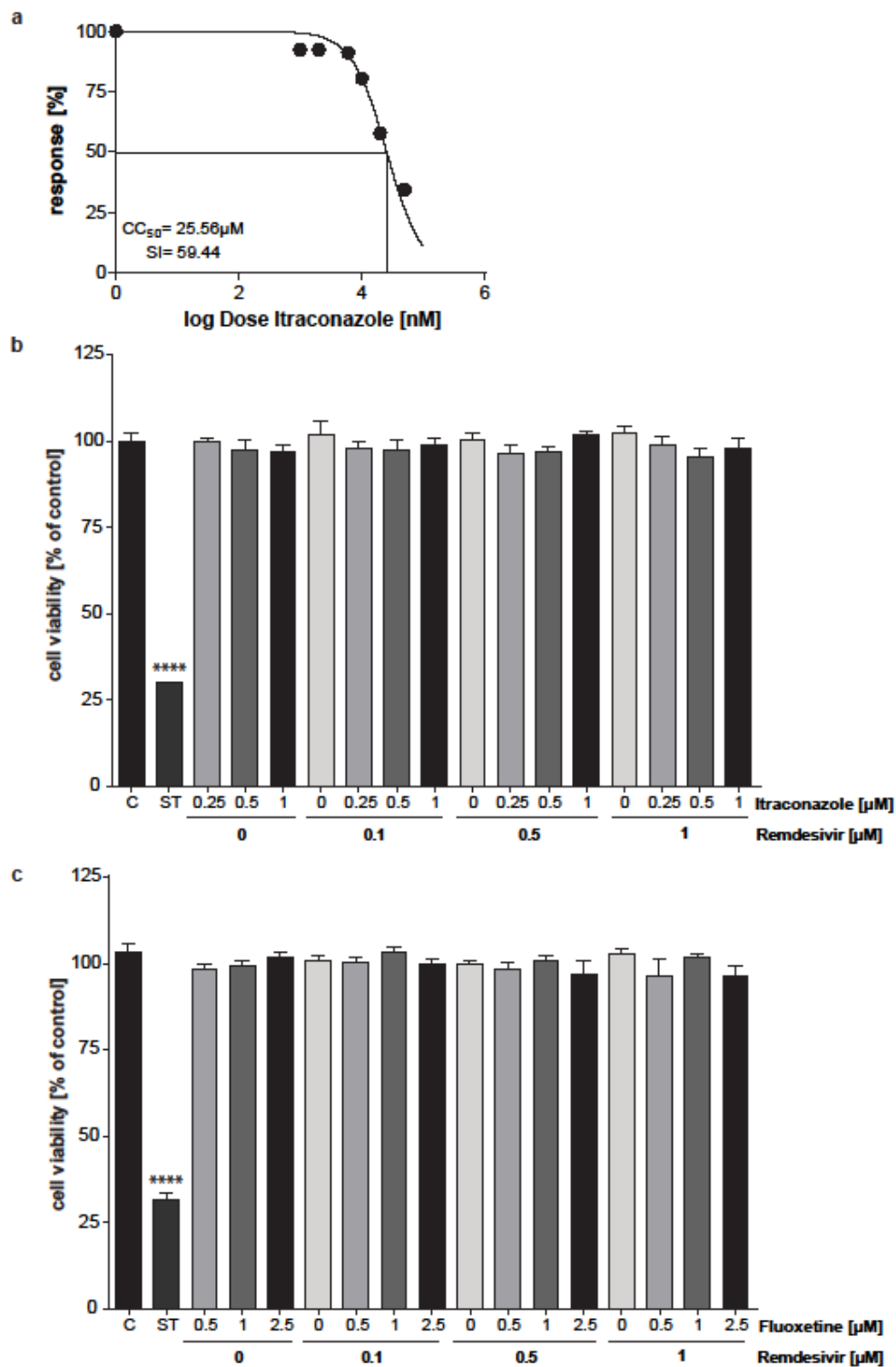
447
448 **SUPPORTING FIGURE 1** Analysis of the cytotoxicity of treatments. (a) Itraconazole, (b)

449 ItraRem, and (c) FluoRem combinatory treatment. Calu-3 cells were treated with the

450   indicated drug combinations for 48 h. Bars display mean percentages of viable

451   cells ± SEM, with mean viability in solvent-treated control cells (C) set to 100%.

452   Staurosporine (ST)- induced cytotoxicity served as a positive control. n = 5, one-way

453   ANOVA followed by Dunnett's multiple comparison test, ****$p < 0.0001$.

454
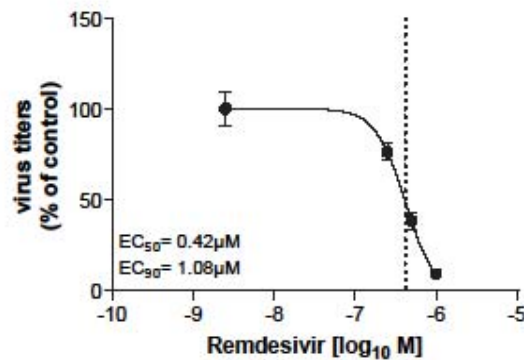
455   **SUPPORTING FIGURE 2** Analysis Dose-Response curve of remdesivir treatments in

456   Calu-3 cells. Calu-3 cells were infected with 0.1 MOI of SARS-CoV-2 for 1 h and treated with

457   the indicated drug combinations for 48 h. Mean percent inhibition ± SEM of SARS-CoV-2

458   replication, with mean virus titer in control cells (treated with the solvent DMSO) set to 100%;

459   n = 5. $LogEC_{50}$ and $LogEC_{90}$ values were determined by fitting a non-linear regression

460   model. (Calu-3: EC50 = 0.42 µM, EC90 = 1.08 µM).